

Wave packet propagation into a negative index medium

Xiaobiao Huang and W. L. Schaich

Department of Physics, Indiana University, Bloomington, Indiana 47405

(Received 20 November 2003; accepted 30 April 2004)

We examine the phenomenon of negative refraction using wave packet propagation. The behavior of a single plane wave incident from vacuum onto a flat surface of a medium with a negative index of refraction is solved analytically. The solution requires matching electromagnetic field components across the interface and produces a reflected and a refracted wave in addition to the incident wave. We form by numerical integration a (Gaussian-weighted) linear combination of these solutions. Pictures and videos that illustrate the resulting wave packet motion are presented for a variety of parameter choices. © 2004 American Association of Physics Teachers.

[DOI: 10.1119/1.1764560]

I. INTRODUCTION

There has recently been intense interest in whether an electromagnetic beam coming from vacuum can undergo negative refraction as it enters a medium. This behavior would be characterized by assigning to the medium a negative index of refraction, n , so that in Snell's law¹

$$\sin \theta_i = n \sin \theta_r, \quad (1)$$

a positive incident angle θ_i and negative n would imply a negative refracted angle θ_r . The beam would not cross over the surface normal as it refracts into the material. The idea that negative refraction might be possible dates back nearly 40 years to some theoretical papers by Veselago.² Only in the last few years have experimental reports appeared,³⁻⁶ which have stimulated a flood of theoretical studies. A subset of this literature is cited here⁷⁻¹³ with a longer list available in Ref. 14. As this rush is (perhaps) subsiding,¹⁵ we offer an heuristic contribution.

Our goal is to develop and present simple model calculations that illustrate the basic phenomenon. The strategy is to construct a localized, drifting wave packet in vacuum and then follow its evolution in space and time as it encounters the flat surface of a negative index medium. Our methods (slightly) extend textbook discussions, such as Chapter 7 in Ref. 16 or Chapter 2 in Ref. 17. The calculations are straightforward and should be easy to reproduce.

In Sec. II we derive the basic equations and introduce the simplified dispersion relation we use inside the negative index medium. The subtle questions about how to match solutions between the vacuum and the negative index medium are explicitly discussed. In Sec. III we present a series of calculations of wave packet motion in one and two dimensions. Various still frames are shown, but videos are an important part of the presentation, which may be accessed through EPAPS.¹⁴ Although one can appreciate what is happening from the algebra and the still frames, the videos really bring the subject to life.

II. WAVE PACKET DERIVATION

We start with the integral

$$e^{-x^2/2a^2} = \int_{-\infty}^{\infty} \frac{d(ka)}{\sqrt{2\pi}} e^{-k^2 a^2/2} e^{ikx}, \quad (2)$$

and introduce several formal changes. Let $x \rightarrow x - ct$, offset the gaussian weight from $k=0$ to $k=k_0$, and replace kct by ωt . Then Eq. (2) becomes

$$e^{ik_0(x-ct)} e^{-(x-ct)^2/2a^2} = \int_{-\infty}^{\infty} \frac{d(ka)}{\sqrt{2\pi}} e^{-(k-k_0)^2 a^2/2} e^{i(kx-\omega t)}. \quad (3)$$

The real part of this complex-valued identity is shown in Fig. 1.

If we take c as the speed of light in vacuum and interpret x and t as position and time, then the left-hand side of Eq. (3) represents a wave packet with a Gaussian envelope that drifts (rigidly) to the right. From the right-hand side of Eq. (3), this result arises from a linear superposition of plane wave solutions in vacuum, each described by wave vector k and (angular) frequency ω with $\omega = kc$. Both the phase velocity, ω/k , and the group velocity, $\partial\omega/\partial k$, equal c .

To describe what happens to the wave packet when it encounters a second, semi-infinite medium, we need only to modify the plane wave factor e^{ikx} . We assume that the flat interface is at $x=0$ with the incident packet coming from $x < 0$, replace $k \rightarrow k_v$ on the right-hand side of Eq. (3), and take

$$e^{-i\omega t} e^{ik_v x} \rightarrow e^{-i\omega t} \begin{cases} e^{ik_v x} - r e^{-ik_v x} & (x < 0) \\ t e^{ik_m x} & (0 < x) \end{cases} \quad (4)$$

where r and t are the reflection and transmission amplitudes, k_v is the incident wave vector in vacuum, and k_m is the transmitted wave vector in the material.

To obtain these parameters, we need to incorporate Maxwell's equations. Initially we will assume one-dimensional (1D) motion along the interface normal x . We choose the $y(z)$ axis along the transverse electric (magnetic) field direction. The real part of Eq. (4) represents $E_y(x,t)/E_0$ and the analogous equation for $B_z(x,t)/B_0$ is obtained by the replacement $-r \rightarrow +r$ and $t \rightarrow tk_m/k_v$. The requirement of continuity of E_y and H_z across $x=0$ yields

$$r = \frac{k_m/k_v - \mu_r}{k_m/k_v + \mu_r}, \quad t = \frac{2\mu_r}{k_m/k_v + \mu_r}, \quad (5)$$

where $\mu_r = \mu/\mu_0$, μ_0 is the permeability of free space, and $\mu(\omega)$ is the permeability of the (presumed isotropic) medium.

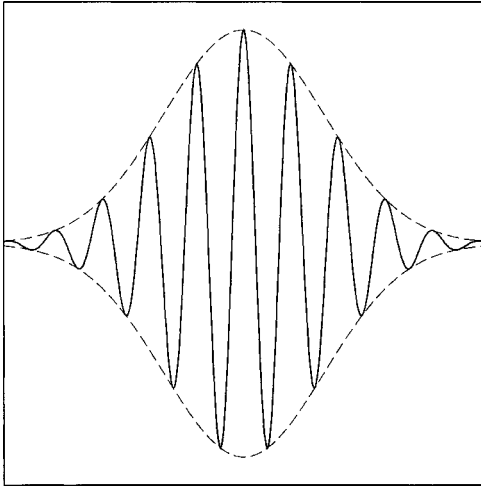


Fig. 1. Gaussian wave packet in vacuum. The solid line is the wave packet and the dashed curves form its Gaussian envelope. As time increases, the wave packet and the envelope move at the common speed c to the right.

There remains the choice of k_m . From Maxwell's equations we obtain

$$k_m^2 = \frac{\omega^2}{c^2} \epsilon_r \mu_r = \frac{\omega^2}{c^2} n^2, \quad (6)$$

where $\epsilon_r = \epsilon/\epsilon_0$, ϵ_0 is the permittivity of free space, and $\epsilon(\omega)$ the permittivity for $x > 0$. The second part of Eq. (6) defines the index of refraction to within a sign. Once we decide how to choose this sign, k_m/k_v can be replaced by n and the result substituted into Eqs. (5) and (4) and integrated over k_v via the extension of Eq. (3).

In this paper we shall explore the implications of the simplifying assumption that

$$\epsilon_r(\omega) = \mu_r(\omega) = 1 - \frac{\omega_p^2}{\omega^2}, \quad (7)$$

$$\mathbf{B} = \begin{pmatrix} -E_0 \\ \omega \end{pmatrix} e^{i(qy - \omega t)} \begin{cases} (-q, p_v, 0) e^{ip_v x} + r(q, p_v, 0) e^{-ip_v x} & (x < 0) \\ t(-q, p_m, 0) e^{ip_m x}, & (x > 0) \end{cases} \quad (12)$$

where the triplets in parentheses represent the x , y , z components. Note that these waves have the same value of ω and q on both sides of the interface. This insures that if a wave is properly matched across $x=0$ when $y=0=t$, then it will be properly matched across $x=0$ for all y and t . The requirement of continuity of E_z and H_y yields

$$r = \frac{p_m/p_v - \mu_r}{p_m/p_v + \mu_r}, \quad t = \frac{2\mu_r}{p_m/p_v + \mu_r}, \quad (13)$$

as the extensions of Eq. (5). For the incident and reflected partial waves we have

$$q = \frac{\omega}{c} \sin \theta_i, \quad p_v = \frac{\omega}{c} \cos \theta_i, \quad (14)$$

where θ_i is the angle of incidence of \mathbf{k}_v .

where ω_p is a fixed (plasma) frequency. For $\omega < \omega_p$ both ϵ_r and μ_r are negative, and as we shall show, the medium has a negative index. We stress that Eq. (7) is introduced as a heuristic simplification. Once it is understood how negative refraction arises for such a case, it will be relatively easy to understand its origin for more realistic constitutive relations. If we substitute Eq. (7) in Eq. (6), we find

$$k_m c / \omega_p = \pm \sqrt{\left(\frac{\omega}{\omega_p} - \frac{\omega_p}{\omega}\right)^2}, \quad (8)$$

that is, two possible k_m for each ω . The appropriate one to use in Eq. (4) is determined by the requirement that the group velocity, $\partial\omega/\partial k_m$, should be positive to guarantee that flux is carried away from the interface and into the medium at $x > 0$. A graphical illustration of the proper choice for k_m is given in Fig. 2.

Equation (8) becomes

$$\frac{k_m c}{\omega_p} = \frac{\omega}{\omega_p} - \frac{\omega_p}{\omega}, \quad (9)$$

which implies that

$$n = 1 - \frac{\omega_p^2}{\omega^2}. \quad (10)$$

We see that n is positive (negative) for ω greater (lesser) than ω_p .

We postpone the numerical evaluation of the 1D wave packet until Sec. III, and instead extend the formal analysis to two-dimensional (2D) motion. We need a 2D k -space integral, so $k_v \rightarrow \mathbf{k}_v = p_v \hat{x} + q \hat{y}$ in Eq. (3). The x - y plane becomes the plane of incidence. We choose the electric field to be perpendicular to this plane and write the extension of Eq. (4) as¹⁸

$$E_z/E_0 = e^{i(qy - \omega t)} \begin{cases} e^{ip_v x} - r e^{-ip_v x} & (x < 0) \\ t e^{ip_m x} & (x > 0). \end{cases} \quad (11)$$

From Faraday's law the corresponding magnetic field is

The remaining question is what to use for p_m . If we combine Eqs. (11) and (12) in Ampere's law, we obtain Eq. (6) or

$$p_m^2 = \frac{\omega^2}{c^2} \epsilon_r \mu_r - q^2. \quad (15)$$

Equation (15) is readily solved for the constitutive relations of Eq. (7), as illustrated in Fig. 3 where we have plotted ω versus the real part of p_m . If p_m^2 is positive, we choose the sign of p_m so that the component of the group velocity along the normal is directed away from the interface; that is, $\partial\omega/\partial p_m > 0$. A new feature that arises is a range of ω where $p_m^2 < 0$, which we call a gap. In the gap p_m is purely imaginary and should be chosen to be positive imaginary in order that the waves in Eqs. (11) and (12) decay as they penetrate

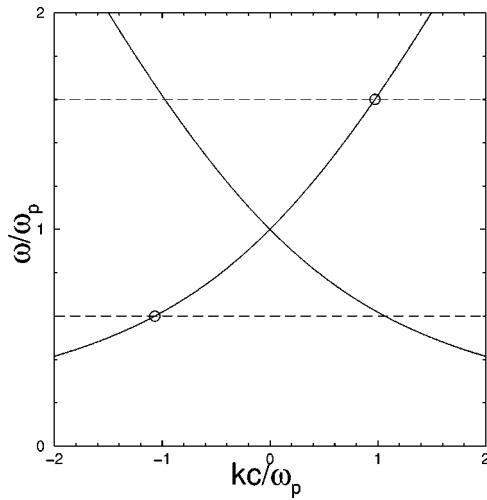


Fig. 2. Dispersion relation for a medium with the constitutive relations of Eq. (7). The horizontal, dashed curves show two possible choices of ω and the small circles mark the appropriate choice of k_m to produce a positive group velocity. Note that the sign of k_m flips when ω passes through ω_p .

into $x > 0$. For this case there is total reflection because $|r| = 1$.

Consider now Snell's law, which arises from the choice of a common $q > 0$:

$$|\mathbf{k}_v| \sin \theta_i = q = |\mathbf{k}_m| \sin |\theta_r|. \quad (16)$$

Our procedure is to first determine the sign of the refraction angle θ_r and then use Eq. (1) to set the sign of n . We recall that for a wave packet built from a continuum of plane waves near \mathbf{k} in an isotropic medium, the phase and group velocities are¹⁹

$$\mathbf{v}_p = \hat{k} \frac{\omega}{k}, \quad \mathbf{v}_g = \hat{k} \frac{\partial \omega}{\partial k}, \quad (17)$$

where $\omega > 0$, \hat{k} is a unit vector along \mathbf{k} , and k is the magnitude of \mathbf{k} . Thus \mathbf{v}_g is parallel (antiparallel) to \mathbf{v}_p when $\partial \omega / \partial k$ is positive (negative). For frequencies above the gap, p_m is positive and the phase and group velocities are parallel for $x > 0$ and directed away from the interface. Hence $\theta_r > 0$, by the usual convention, and $n > 0$. For frequencies below the gap, p_m is negative and the phase and group velocities for $x > 0$ are antiparallel, with only the group velocity directed into $x > 0$. Hence both θ_r and n are negative. Note that the definition for n used here yields the same result as found from Eq. (6) and the construction in Fig. 2.²⁰ The magnitude of n is set simply by $|\mathbf{k}_m|/|\mathbf{k}_v|$, but for its sign we need the direction (although not the magnitude) of \mathbf{v}_g .

We end this section with a brief discussion of extensions of our model. The first possibility is to allow for dissipation. For example in Eq. (7) we could replace $\omega^2 \rightarrow \omega(\omega + i/\tau)$, where $1/\tau$ is a scattering rate. The only formal change this replacement makes in the wave packet calculation is that the rule for choosing p_m is simplified: at all frequencies we want the solution of Eq. (15) with the imaginary part of p_m to be positive. For small $1/\omega_p \tau$, this change does not remove regions where $n < 0$. For larger $1/\omega_p \tau$, a description in terms of Snell's law loses its physical meaning (because n and θ_r acquire significant imaginary parts), although the recipe for

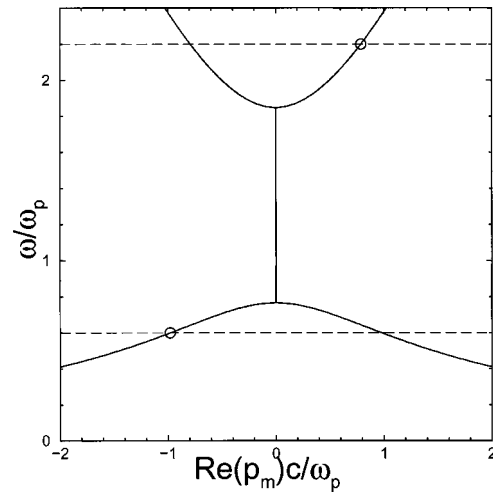


Fig. 3. Dispersion relation for a medium with the constitutive relations of Eq. (7) and a nonzero angle of incidence $\theta_i = 45^\circ$. The method for finding p_m is the same as in Fig. 2 except in the gap between the two branches where $p_m^2 < 0$. Over this range we must choose $p_m = i\sqrt{-p_m^2}$.

p_m remains meaningful and the evolution of the wave packet can be readily calculated. Examples are shown in Sec. III.

Another extension is to allow ϵ_r and μ_r to have a distinct and more complicated (realistic) dependence on frequency. We leave this extension for the interested reader to pursue in detail, and note only that the general prescription we have presented here should still apply. The key for the negative index behavior is that the dispersion relations have the qualitative feature shown in Fig. 2 that $\partial \omega / \partial k$ be negative over a range of ω . Negative refraction also has been observed in photonic crystals and its understanding has developed in parallel to that for the negative index of metamaterial media.²¹⁻²⁷ As the surfaces of constant frequency in \mathbf{k} space distort from spherical, the matching calculation at a surface becomes more complicated, but the principles remain the same.

III. WAVE PACKET EVALUATIONS

We begin with the 1D case and choose $k_0 c / \omega_p = 1/\sqrt{2}$ and $\omega_p a / c = 20$ in Eq. (3). Figure 4 shows the wave packet of the electric field approaching the interface. Note that E_y is continuous, but its slope is discontinuous across $x = 0$. The latter property arises because $\partial E_y / \partial x$ is proportional to B_z , which is discontinuous due to the jump in the permeability. Another remarkable feature is that there is no reflected packet as follows from Eqs. (5) and (10):

$$k_m / k_v = n = \mu_r. \quad (18)$$

This special 1D (normal incidence) property makes it easy to track the motion of the incident wave. The largest positive peak in E_y / E_0 is located at $\omega_p x / c = -30$ when $\omega_p t = -30$. It and the whole incident packet simply shift by $\omega_p \Delta x / c = 10$ for every increment of $\omega_p \Delta t = 10$.

The transmitted packet is more difficult to analyze. In Fig. 5 we show its evolution for smaller increments in time. It is obvious that the points of constant phase are drifting to the left. Their velocity is close to $-c$, which is what one finds by using the index $n_0 = -1$ for the center of the wave packet. The motion of the packet's envelope for $x > 0$ is re-

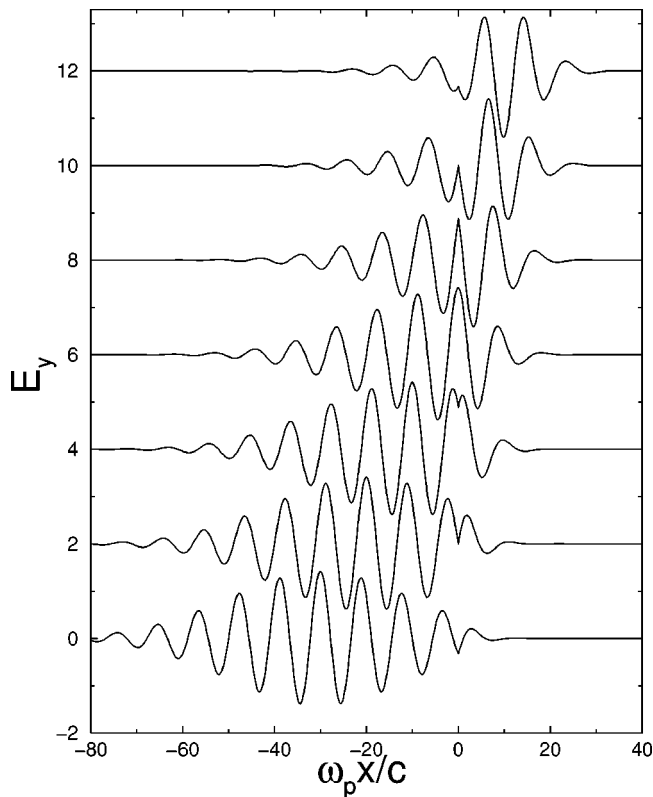


Fig. 4. Wave packets for $\omega_p t$ ranging from -30 to $+30$ in steps of 10 as one moves from the bottom to the top. Each curve is offset by 2 and the maximum $|E_y|$ in the incident packet is $\sqrt{2}$. The vacuum-material interface is at $x=0$.

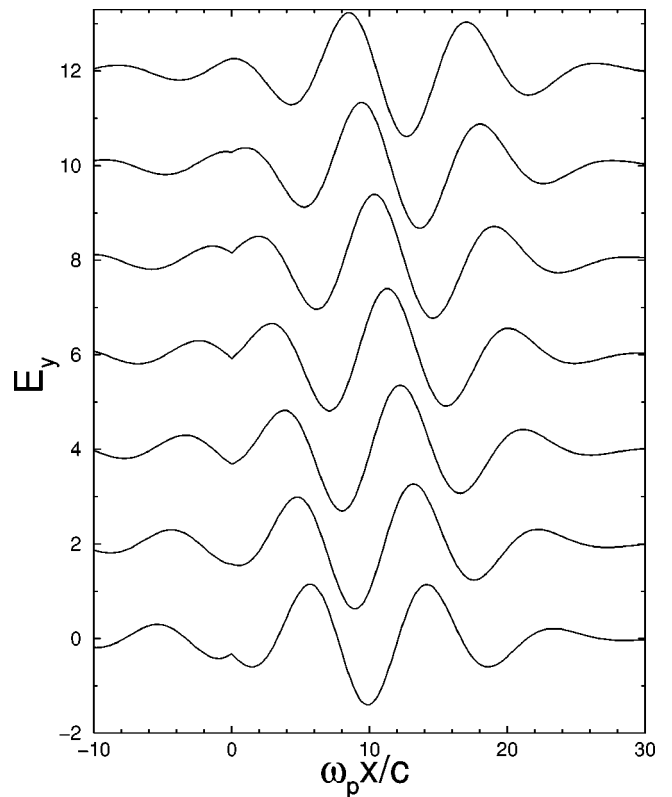


Fig. 5. Same as Fig. 4 except that $\omega_p t$ ranges from $+30$ to $+36$ in steps of 1 as one moves from the bottom to the top.

vealed in Fig. 6. We see that it is to the right but at a reduced speed of approximately $c/3$. If we differentiate Eq. (9), we obtain

$$v_g = \frac{c}{1 + \omega_p^2/\omega^2}, \quad (19)$$

which becomes $c/3$ at $\omega_0/\omega_p = 1/\sqrt{2}$.

We can animate¹⁴ the still frames shown in Figs. 4–6. The backward (forward) motion of the phase (envelope) of the transmitted wave packet is obvious and striking. Note too that over the spatial range exhibited, there is little reduction or distortion of the envelope. In Fig. 6 and a second animation¹⁴ we show how the introduction of a weak dissipation with $\omega_p \tau = 100$ leads to damping of the transmitted packet. The phase and group velocities are scarcely affected.

We now turn to motion in 2D. We want the incident packet to have some asymmetry but to be aligned with the incident direction defined by the unit vector $\hat{k}_v^{(0)}$, which makes an angle θ_i with the surface normal. A general incident wave vector is written as $\mathbf{k} = k_1 \hat{k}_v^{(0)} + k_2 (\hat{z} \times \hat{k}_v^{(0)})$ and its Gaussian weight is $(a_1 a_2 / 2\pi) \exp[-(k_1 - k_v^{(0)})^2 a_1^2 / 2 - (k_2 a_2)^2 / 2]$. We start with $\omega_p a_1 / c = 20$ and $a_2 = a_1 \sqrt{2}$ so that the packet is slightly broader in the direction transverse to its incident trajectory. We further choose $k_0 c / \omega_p = 0.5$ and $\theta_i = 45^\circ$. Note that there are some technical limits to these choices. The p_v and q discussed in Sec. II are given by

$$p_v = k_1 \cos \theta_i - k_2 \sin \theta_i, \quad (20a)$$

$$q = k_1 \sin \theta_i + k_2 \cos \theta_i. \quad (20b)$$

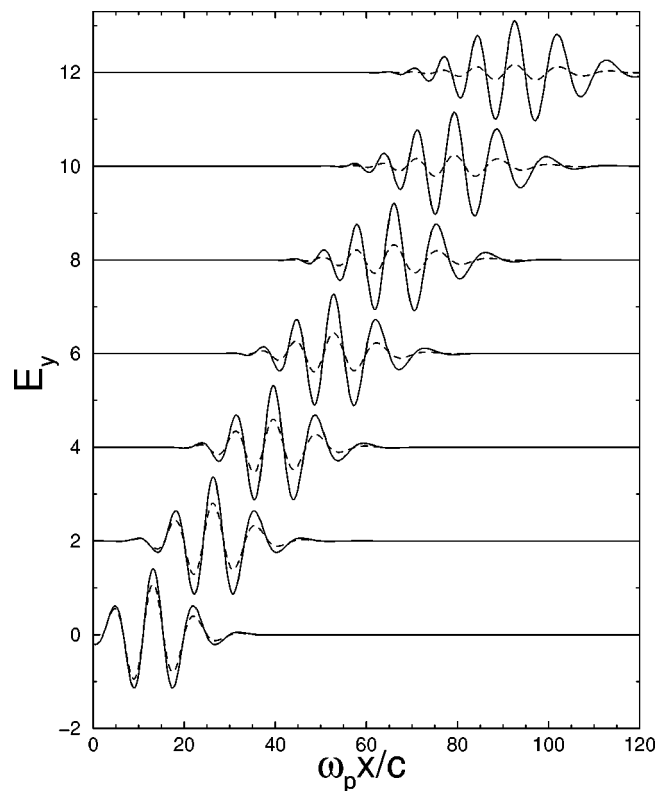


Fig. 6. Same as Fig. 4 except $\omega_p t$ ranges from $+40$ to $+280$ in steps of 40 as one moves from the bottom to the top. For the solid (dashed) curves $1/\omega_p \tau$ equals zero (0.01).

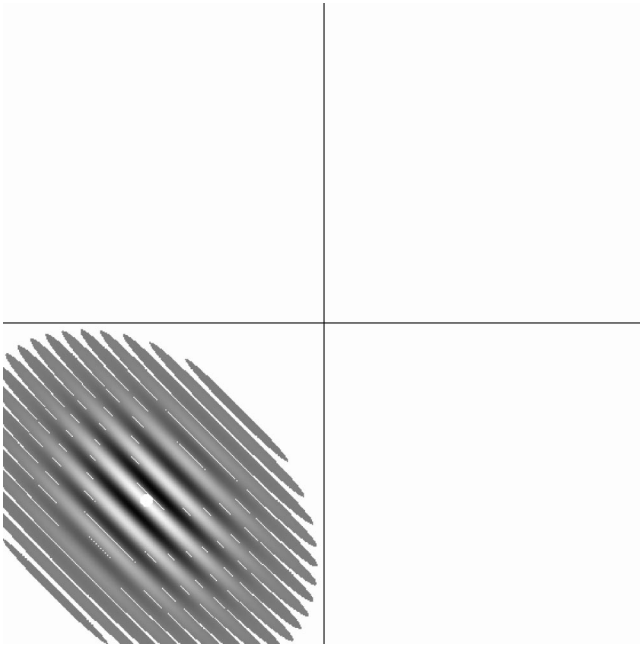


Fig. 7. Single frame for an incident packet at $\omega_p t = -110$ before it reaches the interface which runs vertically through the center. The profile of E_z/E_0 is plotted in greyscale. The bands of constant phase are perpendicular to the direction along which the packet moves and aligned (by design) with the long axis of the packet.

Because the form of the waves we are combining in Eqs. (11) and (12) makes physical sense only if $p_v > 0$, we cannot allow k_1 to be too small or k_2 too large. In turn these constraints imply restrictions on $k_v^{(0)}$, a_1 , and a_2 . We must insure that there is negligible Gaussian weight when $p_v < 0$. Finally, we remark that we shall treat only the polarization analyzed in Sec. II, with E_z normal to the plane of incidence. For the symmetric assumption of Eq. (7), H_z for the orthogonal polarization is, aside from a scale factor, the same function of space and time.

To be specific about what needs to be calculated for 2D motion, we explicitly show the required integrals:

$$E_z(x, y; t)/E_0 = \text{Re} \left[\int \frac{d(k_1 a_1)}{\sqrt{2\pi}} \int \frac{d(k_2 a_2)}{\sqrt{2\pi}} \times e^{-(k_1 - k_v^{(0)})^2 a_1^2 / 2} e^{-k_2^2 a_2^2 / 2} \mathcal{E}_{\mathbf{k}}(x, y; t) \right], \quad (21)$$

where

$$\mathbf{k} = k_1 \hat{k}_v^{(0)} + k_2 (\hat{z} \times \hat{k}_v^{(0)}) = p_v \hat{x} + q \hat{y}, \quad (22)$$

$$\mathcal{E}_{\mathbf{k}}(x, y; t) = e^{i(qy - \omega t)} \begin{cases} e^{ip_v x} - r e^{-ip_v x} & x < 0 \\ t e^{ip_m x} & 0 < x, \end{cases} \quad (23)$$

and $\text{Re}[\dots]$ is the real part of $[\dots]$. Thus the integrands derived in Sec. II are known analytically. They are smooth functions with a rapid cutoff for large values of $|k_2|a_2$ or $|k_1 - k_v^{(0)}|a_1$. The primary numerical challenge is to calculate E_z/E_0 on a sufficiently fine mesh in x , y , and t and then to present the massive data in an understandable form.

In Fig. 7 we show the shape of the incident packet. Be-

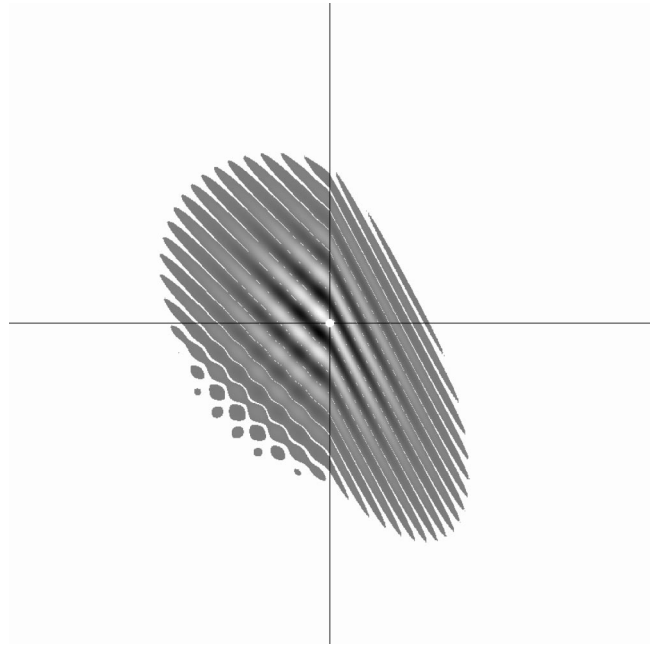


Fig. 8. Single frame at $\omega_p t = 0$ for the packet of Fig. 7 encountering an interface with glass.

cause we are now plotting in 2D, less detail for the packet is shown. Instead of “points,” we shall refer to “bands” of constant phase. This language should be adequate to describe the qualitative features of the packet’s evolution. The vertical axis is the boundary between vacuum and a material (that is, $x=0$), while the horizontal axis is the surface normal. The range of x and y is between -140 and $+139$ times c/ω_p . This field of view is used in all our 2D plots. In the greyscale plot we use white whenever $|E_z/E_0|$ is less than 1% of its maximum value. This choice suppresses noise far from the packet due to inaccurate integrals. However, it also produces dots and strips of white within the packet close to where E_z changes sign. The location and extent of these structures (along a line of $E_z=0$) are arbitrary and should be ignored. There are similar anomalies in the movies where the background is dark. We have superimposed a white disk over the (classical) center of the packet. This disk moves along the classical trajectory. Everything in Fig. 7 (the envelope, the bands of constant phase, and the center disk) moves at the vacuum speed of light until the packet begins to overlap the material for $x > 0$.

We first let this material be glass, with a frequency independent index of $n=1.5$. Figure 8 shows the packet at the instant when the center disk has just reached the interface. The bend in the bands of constant phase across $x=0$ is obvious as the packet undergoes the familiar positive refraction into the glass. Note the smaller wavelength (as evidenced by the width of the phase bands) for $x > 0$, and the initial indication of a reflected packet emerging from the backside of the incident packet.

Figure 9 shows the situation when both the reflected and transmitted packets are fully formed and moving away from the interface. The reflection and transmission amplitudes for $n=1.5$ are $r = -0.11$ and $t = 0.89$, so the reflected packet is considerably weaker than the transmitted packet. There are now two center disks. The one in vacuum moves at c along a line at 45° from the surface normal, while the one in glass

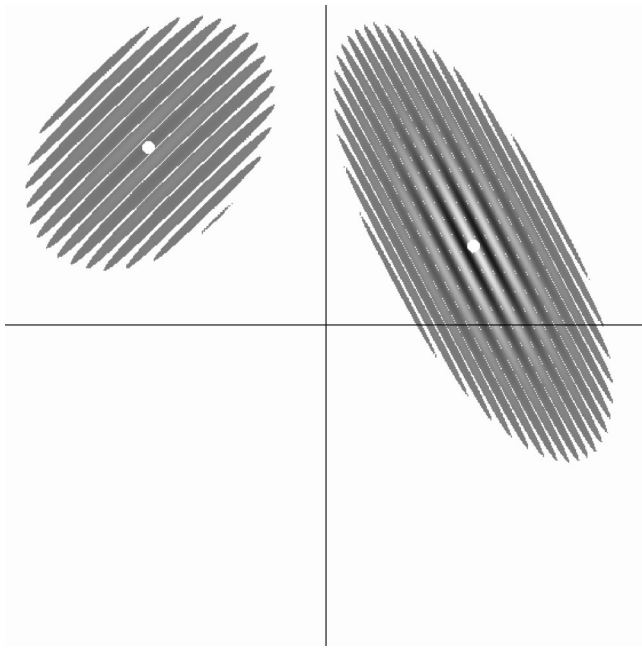


Fig. 9. Single frame at $\omega_p t = +110$ for the packet of Fig. 7 after reflecting from and refracting into glass.

moves at $c/1.5$ along a line inclined at $28.1^\circ = \sin^{-1}[\sin(45^\circ)/1.5]$. In both packets the envelope and phase bands move at a common speed, so the images in Fig. 9 rigidly drift away from $x=0$. The packet's evolution in Figs. 7–9 is available in a third animation.¹⁴ It represents the standard behavior from which we are looking for deviations.

We keep the same incident packet parameters and let the material in $x > 0$ have a negative index. Figure 7 is unchanged, but Fig. 8 is replaced by Fig. 10. On the vacuum side of the interface the packets in Figs. 8 and 10 are quite

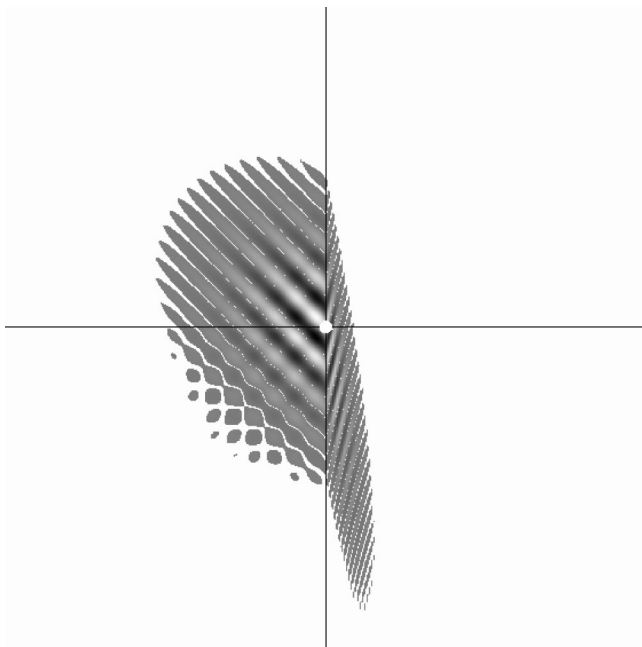


Fig. 10. Single frame at $\omega_p t = 0$ for the packet of Fig. 7 encountering an interface with a negative index. The center frequency is $\omega_0/\omega_p = 0.5$.

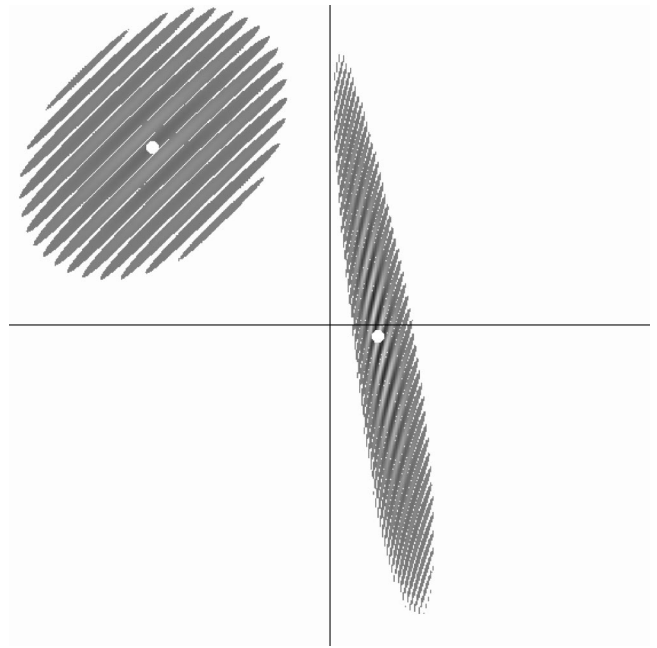


Fig. 11. Single frame at $\omega_p t = +110$ for the packet of Fig. 7 after reflecting from and refracting into a negative index medium. The center frequency is $\omega_0/\omega_p = 0.5$.

similar, but they are dramatically different for $x > 0$. The bands of constant phase are now bent upward (beyond the horizontal) as the interface is crossed, their spacing is smaller, and they are not aligned with an axis of the refracted part of the packet. Furthermore, they move backward as shown in the fourth animation.¹⁴ This qualitative behavior is the same as illustrated in Fig. 5. While the phase bands of the incident packet move (along with its envelope) toward the first quadrant, those of the refracted packet move toward the second quadrant, even though its envelope is moving into the fourth quadrant.

Figure 11 is the analog of Fig. 9. Again although the reflected packets are similar, the refracted packets are distinctly different. For our choice of $\omega_0/\omega_p = 0.5$, the index is $n = -3$, so the phase and group velocities are in opposite directions. From Eq. (17) we find for the negative index medium $v_p = c/3$ and $v_g = c/5$. The angle of refraction is $-13.6^\circ = \sin^{-1}[\sin(45^\circ)/(-3)]$.

In placing the center disks we have made no allowance for a time delay during the reflection/refraction process. The refracted disk starts at the origin at $t=0$ and moves at fixed v_g along the direction of refraction for $t > 0$. The fact that this classical recipe keeps the disk near the visual center of the wave packet is remarkable.

The refracted packet's envelope has been considerably distorted. It still is roughly elliptical, but the ratio of its axes has changed and neither is aligned with the refraction direction, as occurred in Fig. 9. However, the packet persists as a clear entity. In Fig. 12 we show a frame at a much later time, about 40 periods ($2\pi/\omega_0$) after $t=0$. The reflected packet has moved out of the field of view, while the refracted packet continues to drift slowly down into the fourth quadrant. It has broadened significantly compared to Fig. 11, but is still well defined.

We next consider different parameter choices for the incident packet. These values must be chosen with care if we

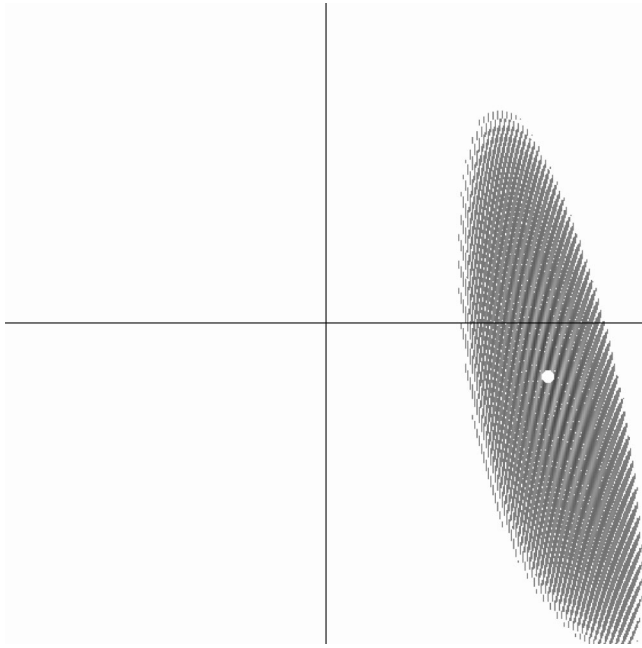


Fig. 12. Single frame at $\omega_p t = +500$ for the packet of Fig. 7 after refracting into a negative index medium. The reflected packet is out of the field of view and the center frequency is $\omega_0/\omega_p = 0.5$.

wish to avoid (undesired) anomalies in the reflected and refracted packets caused by dispersion effects. For instance if a significant number of incident waves are totally reflected (due to their associated values of p_m being imaginary), then the appearance of the refracted packet will exhibit extra distortions. Because both r and t have square root cusps near $p_m^2 = 0$, we should insure that most waves in the packet have neither negative nor even small positive values of p_m^2 . To see how this can be done, consider the condition

$$p_m^2 = 0 = \frac{\omega^2}{c^2} \left(1 - \frac{\omega_p^2}{\omega^2} \right)^2 - \frac{\omega^2}{c^2} \sin^2 \theta_i, \quad (24)$$

which implies that $p_m^2 = 0$ along the pair of curves

$$\omega/\omega_p = (1 \pm \sin \theta_i)^{-1/2}. \quad (25)$$

These curves are plotted in Fig. 13 and represent the boundaries of the gap region within which reflection is total. On the same plot we have drawn several arcs to show how p_v and q vary with the angle of incidence at fixed incident frequency. As ω is increased toward ω_p , the incident beam direction must be moved closer to the normal to avoid the boundary of Eq. (25).

With these considerations in mind, we now choose for the incident packet $\omega_0/\omega_p = 1/\sqrt{2}$, $\theta_i = 20^\circ$, and $\omega_p a_1/c = 30$, but keep $a_2 = a_1\sqrt{2}$. By increasing the packet's width in real space, we reduce its width in wave vector space and also lessen the effects of dispersion. Figure 14 shows the packet at $t=0$. The phase bands form symmetric vees centered on $x=0$. The symmetry arises because $n = -1$. Hence the refracted wavelength equals the incident wavelength, $v_p = c$, and the angle of refraction is -20° . The refracted packet still appears somewhat squashed compared to the incident one because its group velocity is less: $v_g = c/3$.

Figure 15 shows the packet after the refracted part has separated from the interface. Its appearance is qualitatively

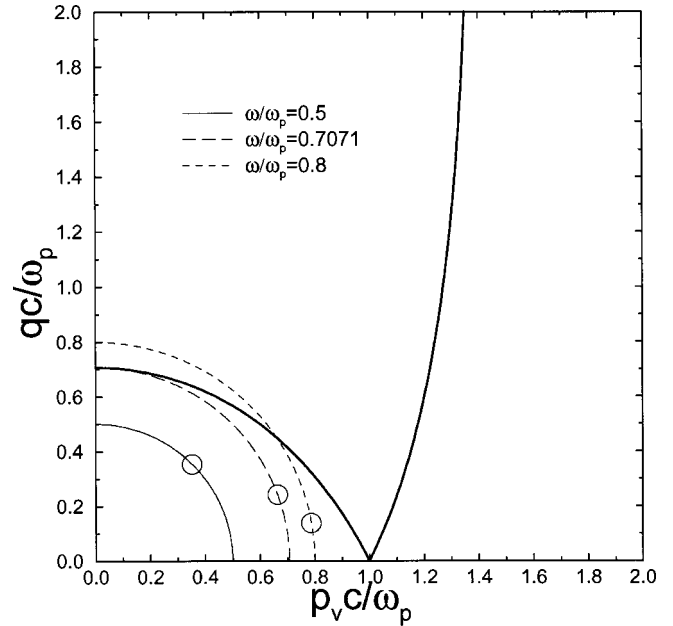


Fig. 13. The definitions of Eq. (14) are used to determine the boundary curves of Eq. (25), which are plotted as thick, solid lines in (p_v, q) space. In between these (where the legends appear) $p_m^2 < 0$ and total reflection occurs. The thinner, circular arcs describe possible values of p_v and q for an incident wave of fixed frequency. The small circles locate the parameter choices for which wave packet calculations are done.

similar to Fig. 11. The striking change is that there is no reflected packet. For $n = -1$, $p_m = -p_v$ so from Eq. (13) $r = 0$, for any angle of incidence! This special behavior at $n = -1$ was noticed by Veselago,² and underlies several of the proposed applications of negative index media.¹⁴ The evolution of the packet is shown in a fifth animation.¹⁴

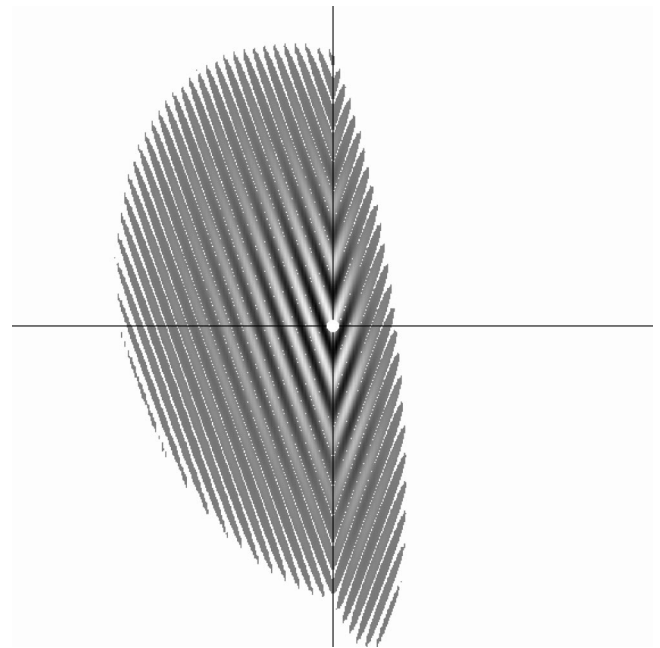


Fig. 14. Single frame at $\omega_p t = 0$ for a packet with $\omega_0/\omega_p = 1/\sqrt{2}$ and $\theta_i = 20^\circ$. The field of view is the same as in earlier (and later) figures, but the packet is 50% wider than before.

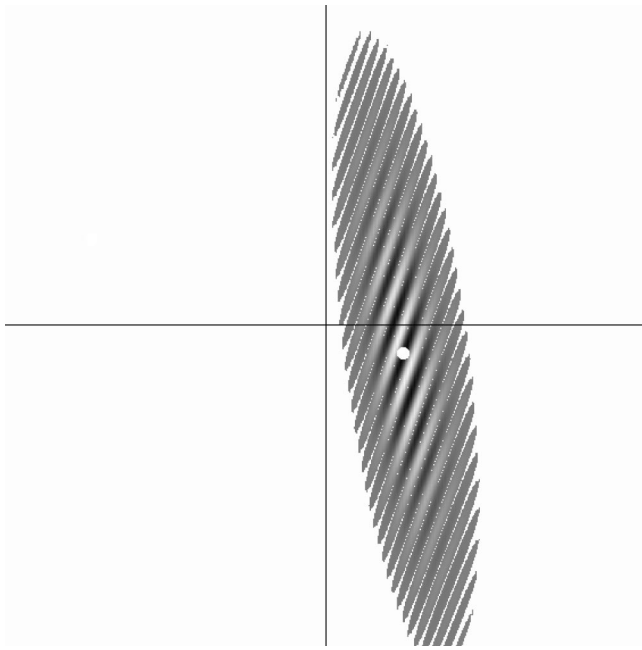


Fig. 15. Single frame at $\omega_p t = +110$ for the same initial conditions as in Fig. 14. The reflected packet is still in the field of view, but has negligible amplitude.

For our final example we use $\omega_0/\omega_p = 0.8$, $\theta_i = 10^\circ$, and $\omega_p a_1/c = 30$ with $a_2 = a_1\sqrt{2}$. For this case $n = -9/16$ so the magnitude of the refracted angle θ_r is greater than θ_i and the wavelength is larger in the negative index medium than in vacuum. Figure 16 shows the packet at $t=0$. Although the wavelength of the refracted piece increases, the spatial extent of the packet in $x > 0$ is less than in $x < 0$ because $v_g/c = 16/41$.

As Fig. 17 illustrates, there is now a weak reflected packet

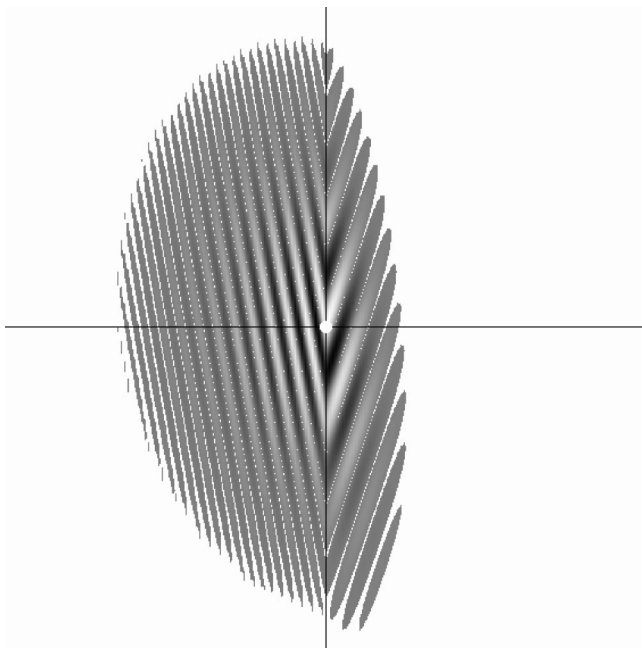


Fig. 16. Single frame at $\omega_p t = 0$ for a packet with $\omega_0/\omega_p = 0.8$ and $\theta_i = 10^\circ$. The incident packet is the same size as in Fig. 14.

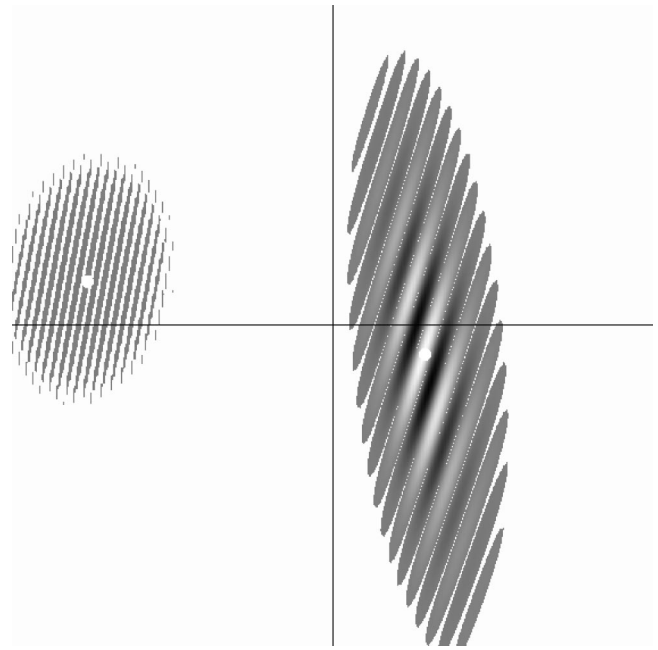


Fig. 17. Single frame at $\omega_p t = +110$ for the same initial conditions as in Fig. 16.

($r^{(0)} = -0.017$) and the refracted packet moves along $\theta_r = \sin^{-1}[\sin(10^\circ)/(-9/16)] = -18.0^\circ$. (See the sixth animation in Ref. 14.)

In summary, we have shown how a wave packet description allows an accessible and transparent picture of negative refraction. On the experimental side, the fundamental new feature is that metamaterials exhibiting a negative index can now be assembled.^{3,5,6} On the theoretical side, which has been our focus, no new principles of optics are needed, only a careful application of known prescriptions. In the examples considered here we have purposely avoided packets that contain (many) waves close to or beyond the total reflection boundary in Fig. 13. For the curious, we have included several additional videos that show what happens when this restraint is ignored, specifically by increasing θ_i at fixed ω_0 .

¹A referee pointed out that the correct (but not common) spelling is Snel. See *Dictionary of Scientific Biography*, edited by Charles Coulston Gillispie (Scribner, New York, 1975), Vol. 12.

²V. G. Veselago, "The properties of materials having simultaneously negative values of the dielectric (ϵ) and the magnetic (μ) susceptibilities," *Sov. Phys. Solid State* **8** (12), 2854–2856 (1967); V. G. Veselago, "The electrodynamics of substances with simultaneously negative values of ϵ and μ ," *Sov. Phys. Usp.* **10** (4), 509–14 (1968); V. G. Veselago, "Electrodynamics of substances with simultaneously negative electrical and magnetic permeabilities," in *Polaritons*, edited by E. Burstein and F. de Martini (Pergamon, New York, 1974).

³R. A. Shelby, D. R. Smith, and S. Schultz, "Experimental verification of a negative index of refraction," *Science* **292**, 77–79 (2001).

⁴Mehmet Bayindir, K. Aydin, E. Ozbay, P. Markoš, and C. M. Soukoulis, "Transmission properties of composite metamaterials in free space," *Appl. Phys. Lett.* **81** (1), 120–122 (2002).

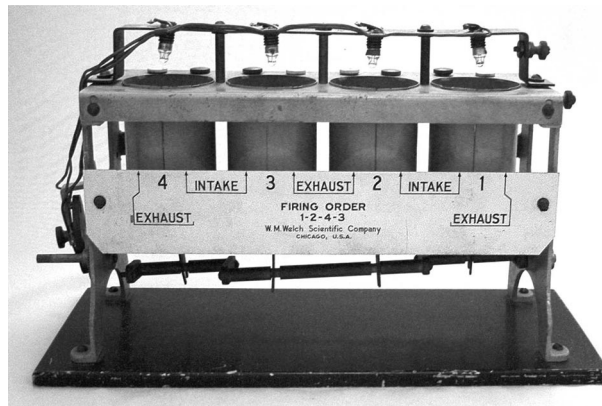
⁵C. G. Parazzoli, R. B. Greegor, K. Li, B. E. C. Koltenbah, and M. Tanielian, "Experimental verification and simulation of negative index of refraction using Snell's law," *Phys. Rev. Lett.* **90** (10), 107401-1–107401-4 (2003).

⁶Andrew A. Houck, Jeffrey B. Brock, and Isaac L. Chuang, "Experimental observations of a left-handed material that obeys Snell's law," *Phys. Rev. Lett.* **90** (13), 137401-1–137401-4 (2003).

⁷J. B. Pendry, "Negative refraction makes a perfect lens," *Phys. Rev. Lett.* **85** (18), 3966–3969 (2000).

⁸Richard W. Ziolkowski and Ehud Heyman, "Wave propagation in media

- having negative permittivity and permeability,” *Phys. Rev. E* **64** (5), 056625-1–056625-15 (2001).
- ⁹P. M. Valanju, R. M. Walser, and A. P. Valanju, “Wave refraction in negative-index media: always positive and very inhomogeneous,” *Phys. Rev. Lett.* **88** (18), 187401-1–187401-4 (2002). These authors have a website (<http://www.utexas.edu/researchemd/nim/>) with a long list of pointers to articles about recent work.
- ¹⁰N. Garcia and M. Nieto-Vesperinas, “Is there an experimental verification of a negative index of refraction yet?,” *Opt. Lett.* **27** (11), 885–887 (2002).
- ¹¹D. R. Smith, D. Schurig, and J. B. Pendry, “Negative refraction of modulated electromagnetic waves,” *Appl. Phys. Lett.* **81** (15), 2713–2715 (2002).
- ¹²J. Pacheco, Jr., T. M. Grzegorzczak, B.-I. Wu, Y. Zhang, and J. A. Kong, “Power propagation in homogeneous isotropic frequency-dispersive left-handed media,” *Phys. Rev. Lett.* **89** (25), 257401-1–257401-4 (2002).
- ¹³R. W. Ziolkowski, “Pulsed and cw Gaussian beam interactions with double negative metamaterial slabs,” *Opt. Express* **11** (7), 662–681 (2003). This paper has movies similar to what we present.
- ¹⁴See EPAPS Document No. E-AJPIAS-72-012408 for additional citations and several movie sequences. A direct link to this document may be found in the online article’s HTML reference section. The document may also be reached via the EPAPS homepage (<http://www.aip.org/pubserv/epaps.html>) or from <ftp.aip.org> in the directory /epaps. See the EPAPS homepage for more information. The movies also are posted at (<http://www.physics.indiana.edu/~schaich/ajp/ajp.html>). A Shockwave player is needed to view the videos.
- ¹⁵D. R. Smith, “The reality of negative refraction,” *Phys. World* **16**, 22–24 (2003).
- ¹⁶J. D. Jackson, *Classical Electrodynamics* (Wiley, New York, 1999).
- ¹⁷S. Brandt and H. D. Dahmen, *The Picture Book of Quantum Mechanics* (Springer, New York, 1995).
- ¹⁸We suppress the taking of only the real part of the expressions in Eqs. (11) and (12).
- ¹⁹We often suppress the subscript on $\mathbf{k}_m \rightarrow \mathbf{k}$ in this paragraph.
- ²⁰For frequencies within the gap, the magnitude of n is too small for θ_r to be a real number. If one wants to determine the sign of n , then lower θ_i (thereby decreasing q and the gap size) until the frequency of interest is no longer in the gap.
- ²¹A metamaterial is an artificial (man-made) composite which on a fine length scale is made of distinct mesoscopic (larger than microscopic) entities. However when probed on a longer length scale, the metamaterial responds as a homogeneous medium. See Refs. 3–6 for how the media are constructed, for example, by stacking an array of circuit boards.
- ²²Hideo Kosaka, Takayuki Kawashima, Akihisa Tomita, Masaya Notomi, Toshiaki Tamamura, Takashi Sato, and Shojiro Kawakami, “Superprism phenomena in photonic crystals,” *Phys. Rev. B* **58** (16), R10096–R10099 (1998).
- ²³Boris Gralak, Stefan Enoch, and Gérard Tayeb, “Anomalous refractive properties of photonic crystals,” *J. Opt. Soc. Am. A* **17** (6), 1012–1020 (2000).
- ²⁴M. Notomi, “Theory of light propagation in strongly modulated photonic crystals: Refraction-like behavior in the vicinity of the photonic band gap,” *Phys. Rev. B* **62** (16), 10696–10705 (2000).
- ²⁵Chiyan Luo, Steven G. Johnson, J. D. Joannopoulos, and J. B. Pendry, “All-angle negative refraction without negative effective index,” *Phys. Rev. B* **65** (20), 201104(R)-1–201104(R)-4 (2002).
- ²⁶S. Foteinopoulou, E. N. Economou, and C. M. Soukoulis, “Refraction in media with a negative refractive index,” *Phys. Rev. Lett.* **90** (10), 107402-1–107402-4 (2003).
- ²⁷S. Foteinopoulou and C. M. Soukoulis, “Negative refraction and left-handed behavior in two-dimensional photonic crystals,” *Phys. Rev. B* **67** (23), 235107-1–235107-5 (2003).



Four Cylinder Gasoline Engine Model. The 1929 catalogue of the W.M. Welch Scientific Company had a complete set of apparatus illustrating the operation of the automobile, including models of the steering gear, chassis, clutch, distributor, universal joint, gear shift, differential, brakes, and this four-cylinder motor that sold for \$25. The valve-lifters, valves and crankshaft can be seen. As the [missing] crank rotates the crankshaft, the pistons go up and down, the valves open and close and the distributor on the end makes the lights flash. The catalogue copy reads “Even the Girls Will Understand How an Auto-Engine Works.” (Photograph and notes by Thomas B. Greenslade, Jr., Kenyon College)